NJC

Accepted Manuscript

This is an *Accepted Manuscript*, which has been through the Royal Society of Chemistry peer review process and has been accepted for publication.

Accepted Manuscripts are published online shortly after acceptance, before technical editing, formatting and proof reading. Using this free service, authors can make their results available to the community, in citable form, before we publish the edited article. We will replace this *Accepted Manuscript* with the edited and formatted *Advance Article* as soon as it is available.

You can find more information about *Accepted Manuscripts* in the Information for Authors.

Please note that technical editing may introduce minor changes to the text and/or graphics, which may alter content. The journal's standard Terms & Conditions and the Ethical guidelines still apply. In no event shall the Royal Society of Chemistry be held responsible for any errors or omissions in this *Accepted Manuscript* or any consequences arising from the use of any information it contains.

ROYAL SOCIETY OF CHEMISTRY

www.rsc.org/njc

Synthesis and visible photocatalytic activities Au@Ag@ZnO triple layer core-shell nanostructure

Mrinmoy Misra, Pawan Kapur, Manoj Kumar Nayak, Madan Lal Singla

Material Research Division, Academy of Scientific & Innovative Research (AcSIR), Central Scientific Instruments Organisation (CSIO), Sector 30 C

Chandigarh, India

Email-id: mrinmoymishra@gmail.com, single_csio@yahoo.co.in

Phone Number: (+91)-9803473089

Fax: (+91)-172-2657267

Abstract:

We report a facile route for the synthesis of Au@Ag@ZnO triple layer core-shell nanostructure with Au as core, Ag as intermediate layer and ZnO as an outer shell. The thickness and surface plasmon resonance (SPR) absorption peak of the Ag shell of Au@Ag bimetal has been controlled by the concentration of $AgNO_3$. In Au@Ag@ZnO nanostructure two major absorption peaks were seen, one due to SPR of Au and other due to the combined effect of Ag and ZnO layer. The photoluminescence study shows that the Au@Ag@ZnO has better charge separation compared to ZnO and Au@ZnO nanostructure. The visible photocatalytic activity for the degradation of methyl orange dye was found to be much higher in case of Au@Ag@ZnO core-shell structure than ZnO or Au@ZnO or TiO_2.

Introduction:

In recent years, nanoparticles of novel metals like Au, Ag, Pd, Cu and Pt have attracted considerable interest because of their unique surface plasmon resonance (SPR), showing dominant optical, electrical and catalytic properties [1]. Studies on bimetallic alloy or core-shell nanoparticles incite interest as they have the capability to enhance the aforementioned properties. For instance, Au-Pt, Au-Cu, Ag-Au and Au-Pd bimetallic alloy nanoparticles show better catalytic properties than the monometallic nanoparticles (NP) [2-5]. Bimetallic alloy nanoparticle show one SPR absorption peak located between two monometallic SPR peaks [6]. In case of Au@Ag bimetallic core-shell nanoparticle, two SPR bands can theoretically and practically be present, by varying the size /shape of the core and the thickness of the shell [7].

Till date, various synthetic routes with various morphologies have been reported for synthesis of Au@Ag core-shell nanoparticles (NPs). For example, Shore and co-workers reported the synthesis of Au@Ag core-shell NPs by digestive ripening method [8]. Zhang et al prepared Au@Ag core-shell NPs by a seeding growth method [9]. Li et al synthesized such water-soluble nanoparticles by using unmodified apoferritin template [10] and Lim et al synthesized DNA-embedded Au@Ag core–shell NPs with controllable silver shell thickness [11]. Pena-Rodriguez et al synthesized Au@Ag core-shell using citrate reduction method [12]. Whereas Zhang et al synthesized Au@Ag using polyelectrolyte multilayerd nanoreactors [13]. Ma et al prepared Au@Ag core shell nonocubes using capping agent like cetyltrimethylammonium bromide (CTAB) or cetyltrimethylammonium chloride (CTAC) with single localized surface plasmon resonance absorption [14]. Guha and co-workers synthesized Au@Ag nanoparticles by synthetic fluorescent dipeptide β-Ala-Trp for Hg(II) sensing [15]. Gong and co-workers synthesized Au@Ag core-shell nanocrystals by varying the shapes of the cores [16]. Yu and co-workers prepared bimetallic Au/Ag core-shell nanorods and found the existence of two longitudinal SPR bands in Au/Ag core_shell nanorods that are due to the contributions from the Ag shell and the Au core [17]. Among the above mentioned methods, the most promising approach is by coating the core with shell layer by successive reduction methods, where we can tune the shell thickness and control the SPR absorption of core and shell individually.

Similarly hollow Au@Ag core-shell nanoparticles prepared by galvanic replacement of an Ag core by Au [18]. The Au@Ag@Au@Ag nanostructure can also be formed by successive reduction of silver salt in the presence of Au@Ag@Au nanoparticles [19]. In case of bimetal core-shell nanoparticle the shell layer usually dominate the optical properties as compare to core [20]. The SPR is strongly affected by the refractive index in the immediate vicinity [21].

By modifying the semiconductor nanostructure with metal or with bimetal, the photocatalytic activity is realized in the visible region, the charge recombination is reduced, and the charge storage is improved. It also shifts the Fermi level to a further negative potential and leads to the formation of a Schottky barrier at the metal-semiconductor interface[22-37]. Li and co-workers synthesized Au@ZnO core-shell structure and studied the photocatalytic properties under UV irradiation [38]. Sun and co-workers synthesized Au-ZnO nanocomposite and applied it as a substrate in surface-enhanced raman scattering (SERS) measurement [39].Misra and co-worker prepared Au@ZnO core-shell structure and studied the photocatalytic degradation of methyl orange (MO) and oxidation of methanol under visible light irradiation[40].

Tsukamoto and co-workers prepared TiO_2 loaded with Au−Ag bimetallic alloy particles and under UV irradiation they efficiently produce H_2O_2 from an O_2-saturated ethanol/water mixture[41]. Zielin´ ska-Jurek and co-workers prepared Au-TiO_2 and Ag/Au-TiO_2 nanoparticles using a water-in-oil microemulsion system and found that the bimetallic samples showed a higher photodegradation rate in visible region than monometallic photocatalysts.[42] Chen and co-worker prepared a Au–Ag-ZnO architecture on indium tin oxide substrate using three-step electrochemical method and study the photocatalytic degradation of methyl orange under UV irradiance[43]. They found a typical absorption peak around 365 nm for the pure ZnO as well as Ag/Au modified ZnO thin film and no visible absorption peak was observed due to presence of Ag/Au.

The literature review revels that no synthesis method has been reported for preparation of Au@Ag@ZnO core-shell structure so far. Keeping in view of this we have developed a novel preparation of Au@Ag@ZnO nanostructure by coating Au@Ag bimetal with ZnO layer. Further we study the growth mechanism of Au@Ag@ZnO core-shell nanostructure. The photocatalytic activities of ZnO nanoparticle, Au@ZnO, Au@Ag@ZnO core-shell nanostructures were evaluated and compared with commercially available TiO_2 powder by the photocatalytic degradation of methyl orange (MO) under visible light irradiance.

Experiment:

Synthesis of gold nanoparticle:

A typical procedure chosen to prepare Au nanoparticle is as follows: 8 ml of 25 mM $HAuCl_4$ was added in 200 ml of deionized (DI) water. Next, freshly prepared 1ml of ice-cold (0.35 M) $NaBH_4$ aqueous solution was quickly added under continuous stirring. The solutions turned yellow to reddish immediately after addition of $NaBH_4$, indicating gold nanoparticle

formation, then 0.5 g of CTAB was mixed in the solution. The molar ratios of Au: BH_4: CTAB was 1:1.77:6.83. The solutions were kept undisturbed for 24 h. The gold nanoparticle colloidal solution was repeatedly washed with ethanol and DI water to remove excess CTAB via centrifugation finally red colour gold nanoparticles was redispersed in 50 ml of DI water and was named as S1.

Preparation of Au@Ag core shell nanoparticle:

From sample S1, four sets of 10 ml gold nanoparticle colloidal suspension were labelled as S2, S3, S4 and S5. 17.6 mM $AgNO_3$ stock solution was prepared in aqueous medium. From this stock solution different amounts of (40 µl, 60 µl, 100 µl and 200 µl) $AgNO_3$ were mixed with S2, S3, S4 and S5 respectively. As a result the Ag^+ ion concentrations were 0.07, 0.105, 0.175, and 0.35µM for sample S2, S3, S4 and S5 repectively. A freshly prepared ice-cold 50 µl (0.35 M) $NaBH_4$ was mixed with each set of solutions so the molar ratio of BH_4: Ag was1:0.04, 1:0.06, 1:0.1 and 1:0.2. The colour of the solution changed from reddish to reddish brown. The prepared Au@Ag core-shell nanostructures were repeatedly washed with DI water to remove unreacted chemicals via centrifugation, and were redispersed in 10 ml of DI water.

Preparation of Au@Ag@ZnO core-shell nanoparticle:

From sample S4, three sets of 3 ml bimetal colloidal suspension were labelled as S6, S7 and S8. 0.1 M zinc acetate and 0.4 M sodium hydroxide stock solution was separately prepared in aqueous medium. From this, 3ml of zinc acetate stock solution were mixed with each set of solution. Simultaneously hydroxide stock solution was added instantly into S6, S7 and S8 and pH of solutions was maintained at 10, 11 and 12 respectively. Finally the ratio of Zn^{2+} and OH^- was maintained at (1:4), (1:8) and (1:12) for sample S6, S7 and S8. Each of the reaction temperature was at 90 °C for about 2 min. Each final product was centrifuged and washed with DI water to remove residual impurities. The residue was dried in vacuum at 60 °C for 6 hrs and the colour of the finally product was dark brown.

Synthesis of ZnO:

For the synthesis of ZnO nanostructure, 20 ml of (0.4 M) sodium hydroxide solution was mixed with 20 ml of (0.1 M) zinc acetate solution under continuous stirring. The resultant solution temperature was maintained at 90 °C for about 2 min. A white-coloured colloidal

solution was found after addition of NaOH. The residue was separated by centrifugation and then washed with DI water to remove unreacted chemicals. The sample thus obtained was named as S9.

Synthesis of Au@ZnO:

In order to synthesise Au@ZnO core-shell nanostructure, 10 ml of previously prepared S1 gold solution was mixed with 20 ml of (0.1 M) zinc acetate solution under vigorous stirring. 20 ml of (0.4 M) sodium hydroxide was added to the above solution under continuous stirring and maintained at a temperature of 90 °C. The colour of the solution turned red to pink after addition of sodium hydroxide. The precipitates were collected after 2 min, and were centrifuged and washed using DI water. This resultant sample was named as S10.

Characterization:

Photoluminescence spectra were measured at room temperature by a Cary Eclipse fluorescence spectrophotometer. The UV-vis absorption measurement of aqueous colloidal solution was measured using Hitachi U-3900 H spectrophotometer. The morphology and structure of nanoparticles studies were carried out by Transmission Electron Microscopy (TEM) using JEM 2100 (JEOL) microscope operating at 120 kV accelerating voltage. Samples were prepared by placing a drop of nanoparticles suspended in water on carbon-coated TEM grids with 300 meshes. The TEM grids were allowed to dry for 10 min at room temperature before analysis.

Photocatalytic activities:

The photocatalytic activities of pure ZnO (S9), Au@ZnO S(10), Au@Ag@ZnO (S6) nanostructures and TiO_2 powder were evaluated by the photocatalytic degradation of methyl orange (MO) in an aqueous medium under visible light. A 150 W Xe lamp with a 390 nm cut-off filter was used as the visible light source. Prior to visible light exposure, 50 ml of (100 mM) MO and 5 mg of catalytic powder (ZnO or Au@ZnO or Au@Ag@ZnO or TiO_2) were magnetically stirred in the dark for 20 min to equilibrate the absorption and desorption of dye molecules. To monitor the degradation process, the absorption of pure MO solution, MO with ZnO, Au@ZnO and Au@Ag@ZnO was recorded after every 10 min at 456 nm.

Results and Discussion:

It is well known that the surface plasmon resonance (SPR) bands of metal nanoparticle depend on the shape, size, structure, composition and dielectric properties of the local environment [44]. The metal nanoparticle shows only a single SPR absorption. In core-shell bimetals, it shows two SPR absorptions, one for the core and the other for the shell. These SPR absorptions are dependent upon shell thickness. After the formation of the shell of certain thickness on the core, the SPR absorption of the core diminishes and shows only one SPR absorption. In order to study the effect of Ag shell thickness on Au core, the SPR absorption has been carried out for samples S2 to S5. It has been found that the pure Au nanoparticles (S1) colloidal solution show SPR characteristic peak located at 533 nm. At lower concentrations of $AgNO_3$ (40 µl) in the S2 solution, the peak position corresponding to gold gets blue shifted to 529 nm and the peak intensity also gets drastically increased, as shown in figure 1. Such a blue-shift of the SPR absorption of Au is consistent with increasing thickness of the Ag shell layer onto the gold core surface as the surface plasmon band position is sensitively dependent upon the coupling between the Au and Ag layers and elemental composition of the metal nanoparticles [6, 15, 17, 45]. With increased the $AgNO_3$ concentration (60 µl) in sample S3 it has been observed that the SPR of Au core gets more blue shifted at 527 nm**.** The Ag shell has been grown on the outer surfaces of Au nanoparticles by the selective reduction of Ag^+ ions and was bound to the surfaces of Au nanoparticles. At higher concentration of $AgNO_3$ (100 µl) in S4 shows two SPR are generated one at 526 nm and the other at 425 nm which corresponds to gold core and silver shell respectively. So we can reveal that this was the optimum $AgNO_3$ concentration for the generation two SRP peaks. With a further increase of $AgNO_3$ concentration in S5, the peak corresponding to Au core gets diminished shoulder at ~523 nm and the peak corresponding to Ag shell becomes prominent at 420 nm. The detail SPR absorption values has been given in the supporting information (table S1). Therefore, when the Ag shell is sufficiently thick, the Au core SPR peak becomes very weak. As a result, the absorption spectrum shows one distinct peak from the outer surface of Au@Ag at a shorter wavelength of 420 nm. The SPR absorption of Au core of Au@Ag bimetal gets blue shifted as compared to pure Au

nanoparticle. Since we know that the ionic potential of Au (9.1 eV) is higher than that of Ag (7.55 eV), due to an electronic interaction between Au core and the Ag shell, the electrons will get transferred from Au core to the Ag shell, resulting a reduction in electron density and blue shifting in the SPR of Au core. When bimetal nanoparticles were comes in contract with Zn^+ and OH^- ions in the reaction media the ZnO nucleation start on the surface Ag layer. After the first nucleation formation, the bimetal nanoparticle particles begin to grow by diffusion of the reactants through the solution to the surface of the growing particles. In case of sample S6 the pH of solution was 10 and Au@Ag@ZnO nanoparticle shows two broad absorptions have been observed one at 506 and other at 428 nm. The first corresponds to SPR of Au, and the second is related to combined absorption of Ag and ZnO layer. Further increase the pH value (11-12) of solution the solubility of zinc species get enhance in the reaction media, as a result the growth of relatively accumulated and larger Au@Ag@ZnO nanoparticle with thick ZnO shell was observed[46]. The effect of pH value also reflects in the absorption of Au@Ag@ZnO nanoparticle. At higher pH value the absorption of ZnO shell becomes prominent than the Au@Ag absorption. The pure ZnO nanostructure shows absorption at 358 nm. The Au@ZnO shows two absorptions, one at 377 nm and the other at 516 nm. The absorption peak of ZnO shell in the Au@ZnO core-shell structure undergoes a red-shift in comparison to pure ZnO nanoparticle, which attributes the formation of ZnO nucleation layer on the surface of Au nanoparticle. The absorption of Au is attributed to the surface plasmon resonance (SPR) response of Au cores, and a significant blue-shift against pure Au nanocrystals is observed as the surface plasmon generated electrons in Au get transferred to the conduction band of ZnO. The detail absorption of samples S6-S8 has been given in the supportive information (table S2).

After addition of $AgNO_3$ in the Au nanoparticle solution, the silver ion (Ag^+) comes into contact of Au nanoparticle. When the strong reducing reagent $NaBH_4$ is added into the solution, the Ag^+ gets reduced to Ag^0 and a nucleation layer of Ag is formed on the surface of Au seed [13]. The shell thickness of Ag in Au@Ag core-shell nanoparticles depend upon the concentration of $AgNO_3$ in the solution as shown in the TEM image figure 2(a to e). For the synthesis of Au@Ag@ZnO nanoparticle, zinc acetate and sodium hydroxide were mixed in bimetal solution. A thin layer of ZnO was formed on the surface of Ag, as the ratio of Zn^+/OH^- is relatively high in the solution which also helps in crystal aggregation of ZnO under the driving forces of surface energy and electrostatic force. The TEM image and its size distribution has been given in figure 2(f-h). The TEM image and size distribution of

sample S9 and sample S10 also shown in figure 2 (i and j). The schematic representation of the growth mechanism of Au@Ag@ZnO core-shell nanostructure shown in the figure 3. The size distribution range and shell thickness for core-shell material has been given in supporting information (table S3).

To study the electron transfer mechanism the photoluminescence (PL) characteristics of the ZnO, Au@ZnO and Au@Ag@ZnO nanoparticles were carried out at room temperature with an excitation wavelength of 330 nm. It has been observed that ZnO shows the emission band centered at 378 nm and no emission band in the visible region as shown in the figure 4. This UV emission band attributed to the near edge band emission of ZnO. The Au@ZnO and Au@Ag@ZnO have nearly same emission at 387 nm but lower emission intensity than ZnO. The Au@Ag@ZnO possesses better charge separation behaviour than ZnO and Au@ZnO. As soon as the metal nanoparticles come in contact with ZnO, it induces bending of energy band of ZnO. At the interface, a schottky barrier is formed, leading to an upward bending of the energy band of ZnO. Since the work functions of Ag (4.26 eV) and Au (5.1 eV) are lower than that of ZnO (5.3 eV), electrons will get transferred from metal to ZnO until the Fermi level of both come at the same level [47-49].When Au@Ag bimetal interacts with ZnO, a new Fermi energy level is formed at the interface of semiconductor-bimetal junction to create a stable state. The free electrons present in the bimetal will flow towards ZnO until the Fermi level of both comes to the same level. The overall Fermi level of Au@Ag@ZnO moves upwards as compared to pure ZnO. Schematic energy-band diagrams of Au@ZnO, Ag@ZnO, and Au@Ag@ZnO nanostructures are shown in figure 5 (a, b and c). The electron transfer path way of Au@Ag@ZnO under UV excitation was shown in the figure 5 (d).

To study the photocatalytic activities of ZnO (S9), Au@ZnO (S10), Au@Ag@ZnO (S6) nanostructures and commercially available TiO_2 powder, they were tested for methyl orange degradation process under visible illumination. Methyl orange (MO) showed single absorption peak at 456 nm in the visible region. To compare the photocatalytic activity more quantitatively, we have monitored the change in MO concentration (C), relative to the initial concentration (C_0). The figure 6(b) shows the degradation curve for all the samples estimated as C/C_0 versus time. The degradation efficiency η (%) could be calculated as

$$\eta\,(\%) = \frac{C_0 - C}{C_0} \times 100 \qquad (1)$$

where C_0 is the initial concentration of dye and C is the concentration after photo degradation. In the absence of any catalyst, MO shows no change in absorption intensity up to 50 min. The Au@ZnO (S10) core-shell NPs show better photocatalytic activity as compared to pure ZnO

(S9) and TiO_2 powder. It degrades about 53% of MO, while pure ZnO degrades only 8% of MO. This can be attributed to the presence SPR generated electron of Au core. Furthermore, Au@Ag@ZnO (S6) degrades about 93% of MO and shows superior photocatalytic activity than ZnO, Au@ZnO NPs and TiO_2. The specific schematic diagram of MO degradation using Au@Ag@ZnO is illustrated in figure 6(a). The Au@Ag bimetal acts as a source of two SPR generated electrons under visible illumination. The SPR generated e^- transfers to the conduction band of ZnO, where it gets trapped by electron acceptors such as adsorbed O_2 to produce superoxide radical anions $O_2^{\cdot -}$. And then, the $O_2^{\cdot -}$ radicals can further react with H_2O to produce H_2O_2 in aqueous solution. Further H_2O_2 react with electrons to form $\cdot OH$ radical which is responsible for degradation of MO as it happen in case of TiO_2 nanospheres decorated by Au nanoparticles [50]. The photocatalytic degradation of MO can be summarized by the following reactions.

$$e_{CB}^- + O_2 \rightarrow O_2^{\cdot -} \quad (2)$$

$$O_2^{\cdot -} + H_2O \rightarrow HO_2^{\cdot} + OH^- \quad (3)$$

$$HO_2^{\cdot} + HO_2^{\cdot} \rightarrow H_2O_2 + O_2 \quad (4)$$

$$H_2O_2 + e_{CB}^- \rightarrow \cdot OH + OH^- \quad (5)$$

$$Dye + \cdot OH \rightarrow Degradation\ products \quad (6)$$

Conclusion:

In summary, we have successfully demonstrated a facile approach of preparation of Au@Ag@ZnO nanoparticles in aqueous medium. In case of Au@Ag nanoparticle, the shell thickness of Ag layer could be tuned by controlling the concentration of $AgNO_3$. The SPR of Au and Au@Ag suppressed the near edge band emission of ZnO and reduced the charge recombination. The Au@Ag@ZnO showed better visible photocatalytic behaviour than Au@ZnO and ZnO.

Acknowledgments: The authors acknowledge CSIR for research fellowships and supports extended for this work. The authors also acknowledge Mr. P. Chakraborty for his helpful discussion.

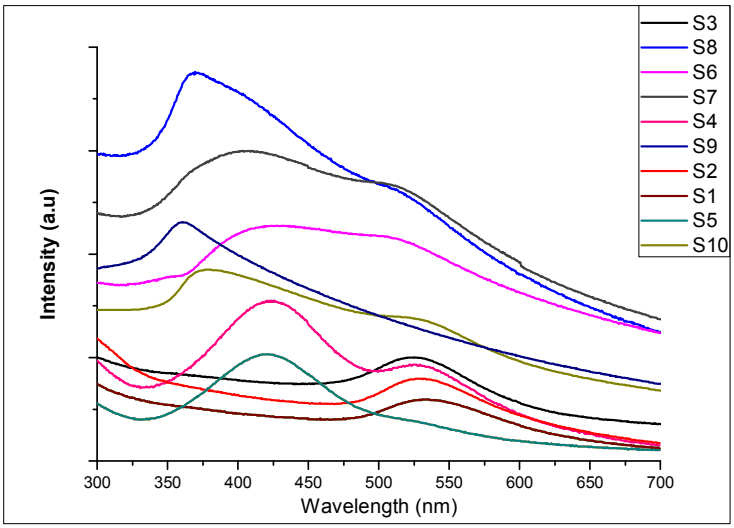

Figure 1. UV-vis absorption spectra of Au, Au@Ag and Ag@Au@ZnO nanoparticles

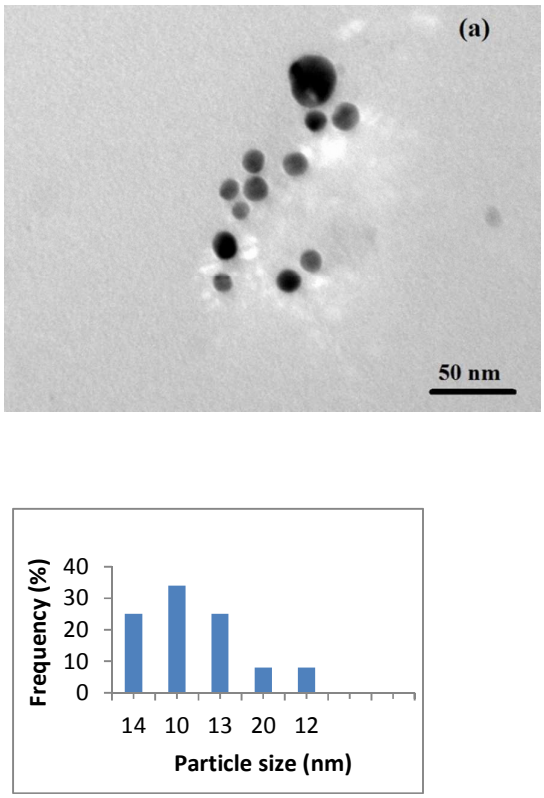

Figure 2 (a) TEM image of Au (sample S1) nanoparticle and its size distribution histogram

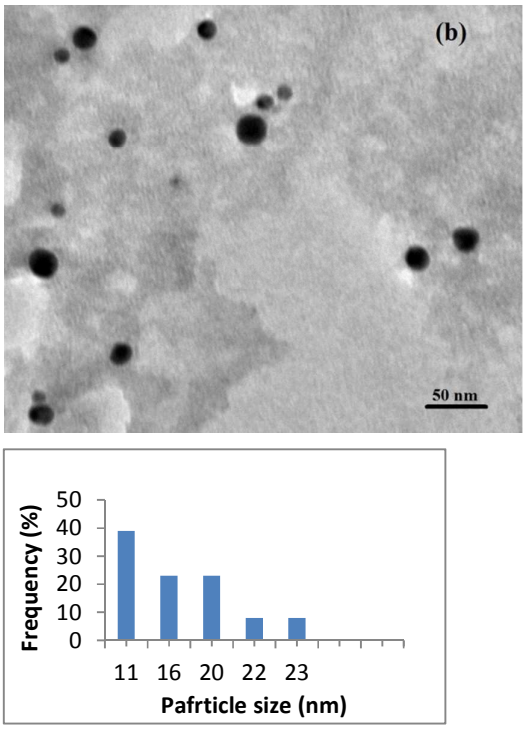

Figure 2 (b) TEM image of Au@Ag (sample S2) nanoparticle and its size distribution histogram

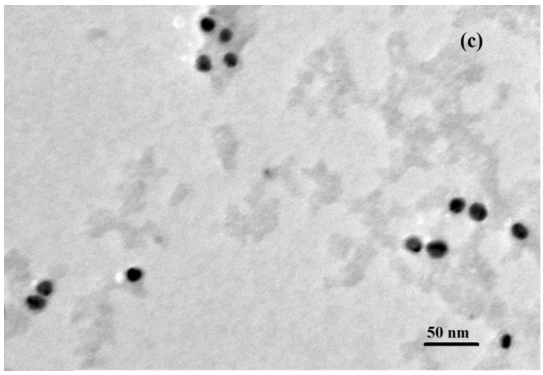

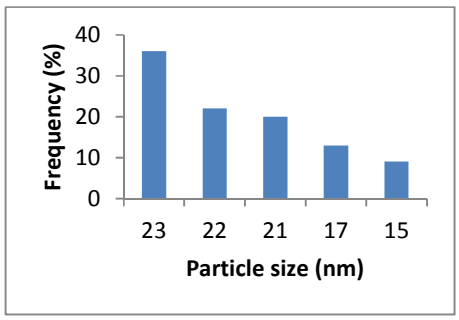

Figure 2 (c) TEM image of Au@Ag (sample S3) nanoparticle and its size distribution histogram

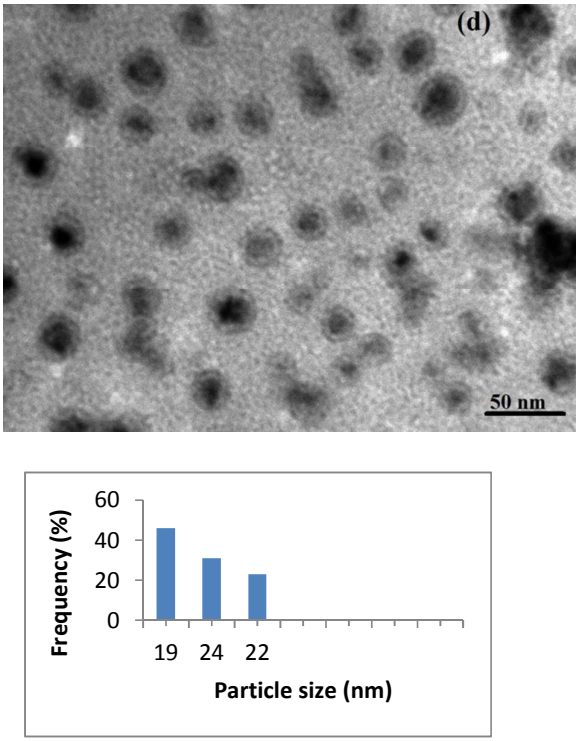

Figure 2 (d) TEM image of Au@Ag (sample S4) nanoparticle and its size distribution histogram

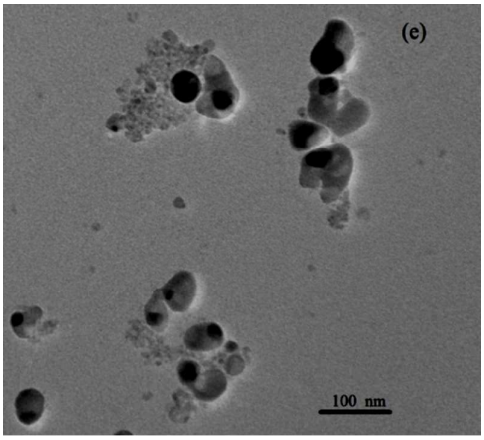

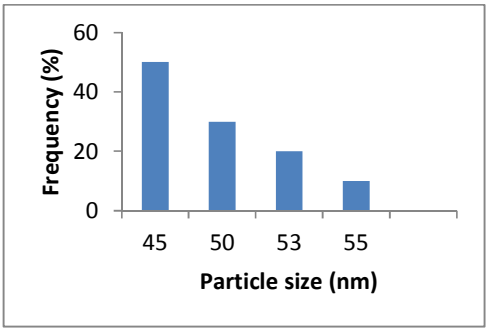

Figure 2 (e) TEM image of Au@Ag (sample S5) nanoparticle and its size distribution histogram

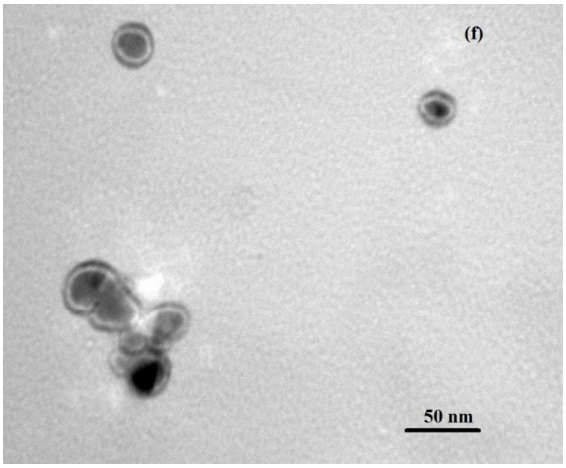

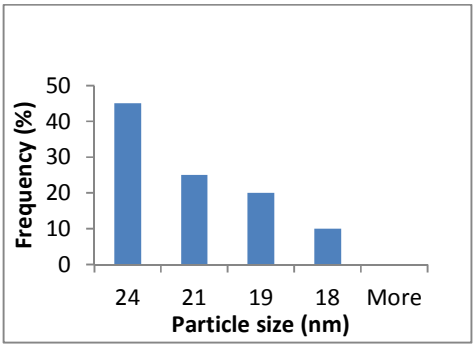

Figure 2 (f) TEM image of Au@Ag@ZnO (sample S6) nanoparticle and its size distribution histogram

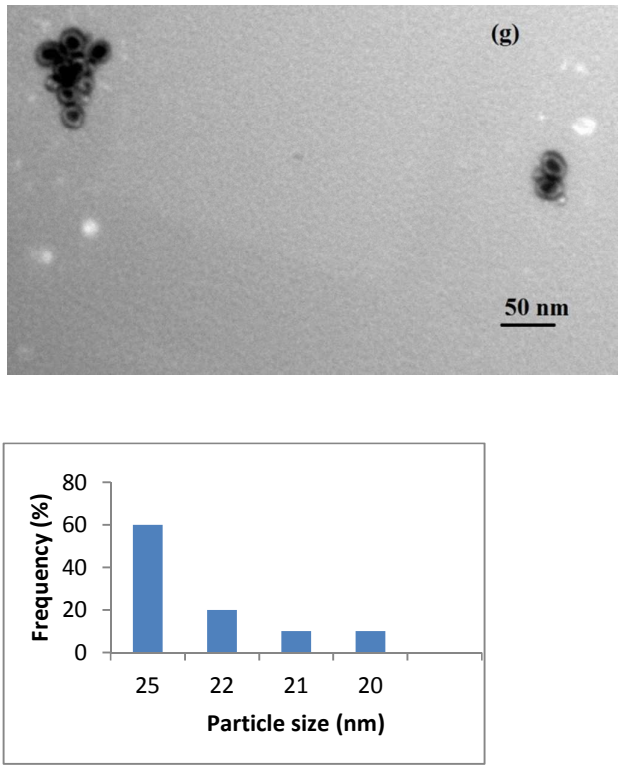

Figure 2 (g) TEM image of Au@Ag@ZnO (sample S7) nanoparticle and its size distribution histogram

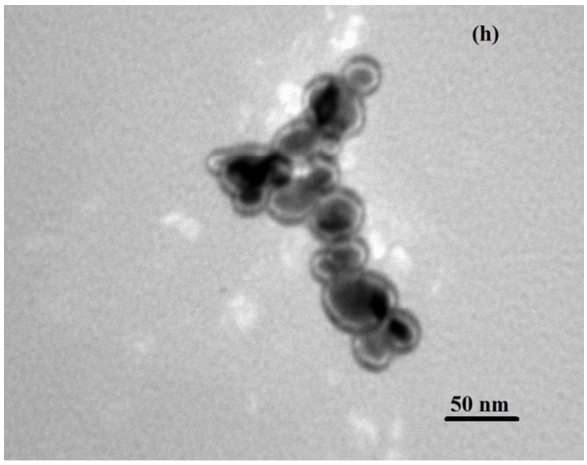

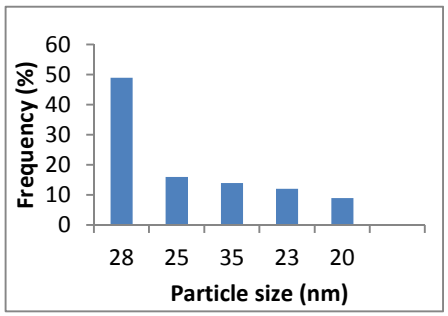

Figure 2 (h) TEM image of Au@Ag@ZnO (sample S8) nanoparticle and its size distribution histogram

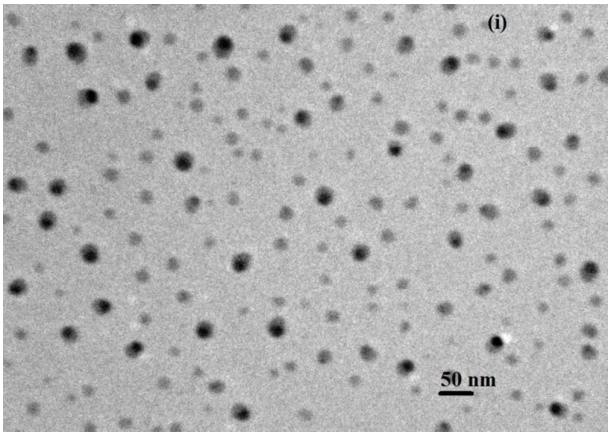

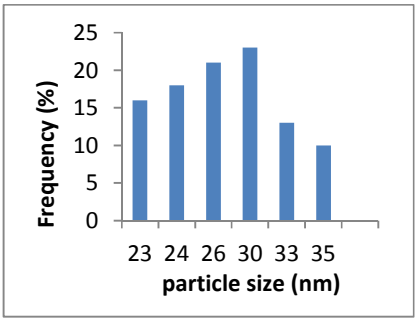

Figure 2 (i) TEM image of Au@ZnO (sample S9) nanoparticle and its size distribution histogram

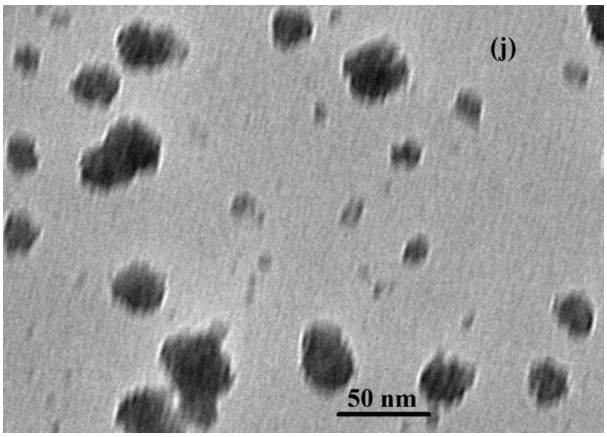

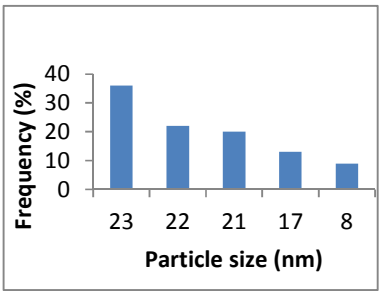

Figure 2 (j) TEM image of ZnO (sample S10) nanoparticle and its size distribution histogram

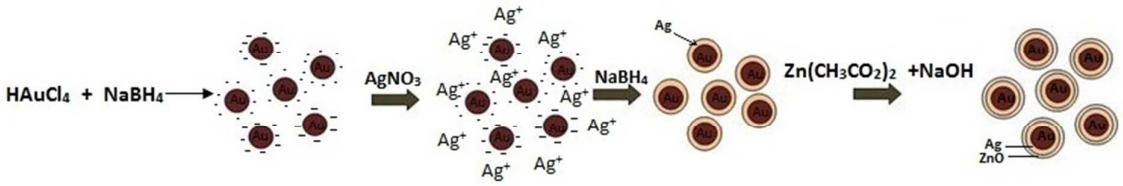

Figure 3 Schematic representation of growth mechanism of Au@Ag@ZnO core-shell nanostructure

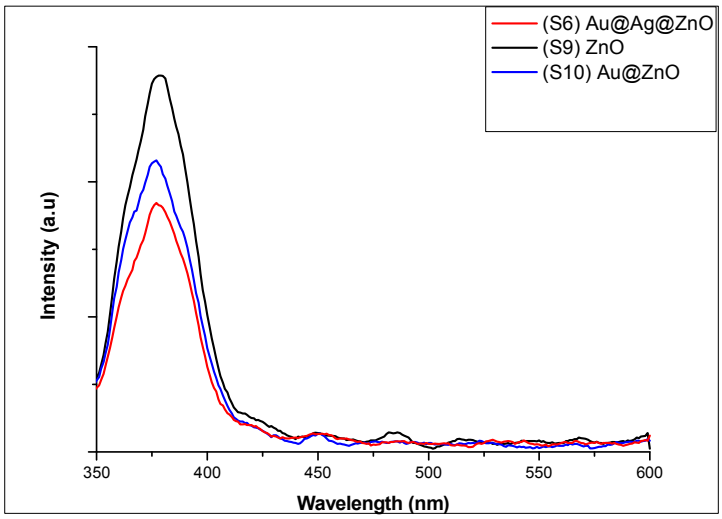

Figure 4. Photoluminescence spectra of ZnO, Au@ZnO and Au@Ag@ZnO nanoparticles

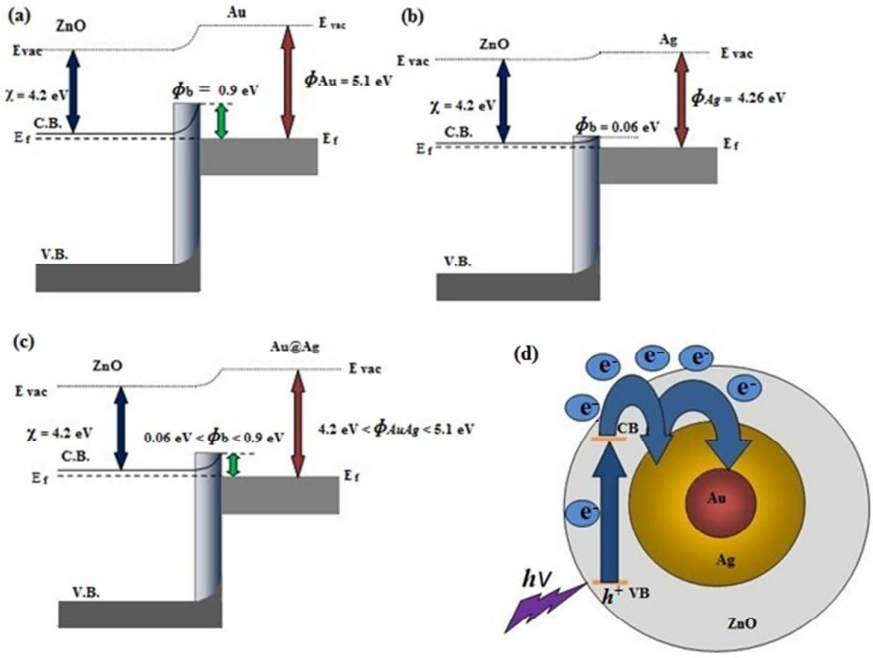

Figure 5. Schematic energy-band diagrams for (a) Au@ZnO, (b) Ag@ ZnO, and (c) Au@Ag@ZnO nanostructure, where E_{vac}, E_f, Φ_M, Φ_b, and χ denote vacuum level, Fermi level, work function of metal, Schottky barrier height, and electron affinity of ZnO conduction band respectively (in eV) and (d) electron transfer pathway between bimetal and ZnO.

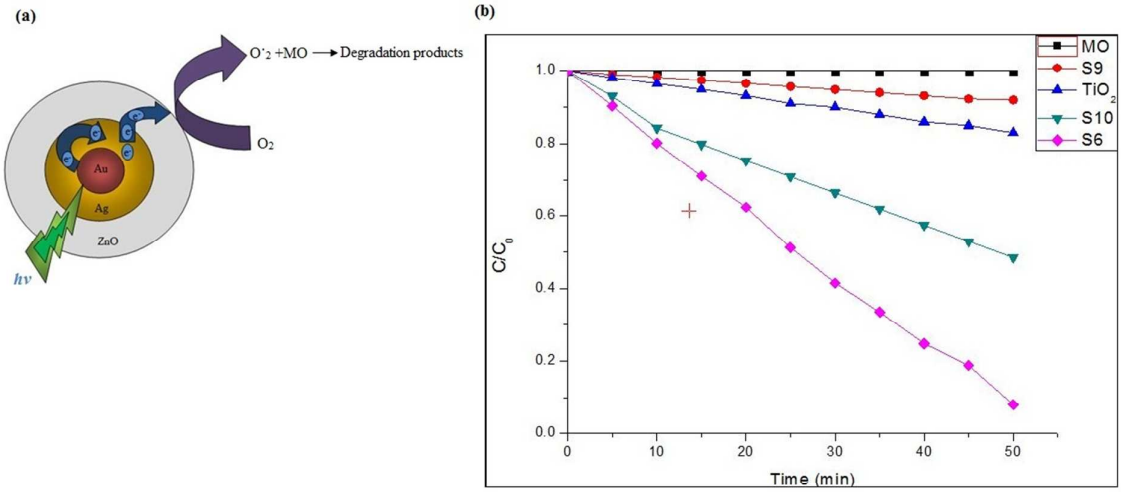

Figure 6. Schematics of proposed visible light induced photocatalytic mechanism of Au@Ag@ZnO core-shell nanostructure (a) Kinetics of MO photo degradation by ZnO (S9), Au@ZnO (S10), Au@Ag@ZnO (S6) and TiO_2 (b)

Reference:

1. S. Guo and E. Wang, *Nano Today*, 2011, 6, 240-264.
2. Z. Zhang, Y. Wang and X. Wang, *Nanoscale*, 2011, 3, 1663-1674.
3. R. J. Chimentão, F. Medina, J. L. G. Fierro, J. Llorca, J. E. Sueiras, Y. Cesteros and P. Salagre, *Journal of Molecular Catalysis A: Chemical*, 2007, 274, 159-168.
4. A.-Q. Wang, J.-H. Liu, S. D. Lin, T.-S. Lin and C.-Y. Mou, *Journal of Catalysis*, 2005, 233, 186-197.
5. M. B. Cortie and A. M. McDonagh, *Chemical Reviews*, 2011, 111, 3713-3735.
6. S. Liu, G. Chen, P. N. Prasad and M. T. Swihart, *Chemistry of Materials*, 2011, 23, 4098-4101.
7. O. Peña-Rodríguez and U. Pal, *Nanoscale research letters*, 2011, 6, 1-5.
8. M. S. Shore, J. Wang, A. C. Johnston-Peck, A. L. Oldenburg and J. B. Tracy, *Small*, 2011, 7, 230-234.
9. Y. Yang, J. Shi, G. Kawamura and M. Nogami, *Scripta Materialia*, 2008, 58, 862-865.
10. T. Li, S. Chattopadhyay, T. Shibata, R. E. Cook, J. T. Miller, N. Suthiwangcharoen, S. Lee, R. E. Winans and B. Lee, *Journal of Materials Chemistry*, 2012, 22, 14458-14464.
11. D.-K. Lim, I.-J. Kim and J.-M. Nam, *Chemical Communications*, 2008, 0, 5312-5314.
12. O. Pena-Rodriguez and U. Pal, *Nanoscale*, 2011, 3, 3609-3612.
13. X. Zhang, H. Wang and Z. Su, *Langmuir*, 2012, 28, 15705-15712.
14. Y. Ma, W. Li, E. C. Cho, Z. Li, T. Yu, J. Zeng, Z. Xie and Y. Xia, *ACS Nano*, 2010, 4, 6725-6734.
15. S. Guha, S. Roy and A. Banerjee, *Langmuir*, 2011, 27, 13198-13205.
16. J. Gong, F. Zhou, Z. Li and Z. Tang, *Langmuir*, 2012, 28, 8959-8964.
17. K. Yu, G. You, L. Polavarapu and Q.-H. Xu, *The Journal of Physical Chemistry C*, 2011, 115, 14000-14005.
18. Y. Sun and Y. Xia, *Journal of the American Chemical Society*, 2004, 126, 3892-3901.
19. B. Rodriguez-Gonzalez, A. Burrows, M. Watanabe, C. J. Kiely and L. M. Liz Marzan, *Journal of Materials Chemistry*, 2005, 15, 1755-1759.
20. A. J. Logsdail and R. L. Johnston, *The Journal of Physical Chemistry C*, 2012, 116, 23616-23628.
21. M. B. Cortie, A. Dowd, N. Harris and M. J. Ford, *Physical Review B*, 2007, 75, 113405.
22. N. Udawatte, M. Lee, J. Kim and D. Lee, *ACS Applied Materials & Interfaces*, 2011, 3, 4531-4538.
23. Y.-M. Chang, M.-L. Lin, T.-Y. Lai, H.-Y. Lee, C.-M. Lin, Y.-C. S. Wu and J.-Y. Juang, *ACS Applied Materials & Interfaces*, 2012, 4, 6676-6682.
24. G. Sinha, L. E. Depero and I. Alessandri, *ACS Applied Materials & Interfaces*, 2011, 3, 2557-2563.
25. M. D. L. Ruiz Peralta, U. Pal and R. S. Zeferino, *ACS Applied Materials & Interfaces*, 2012, 4, 4807-4816.
26. Y. Zheng, C. Chen, Y. Zhan, X. Lin, Q. Zheng, K. Wei and J. Zhu, *The Journal of Physical Chemistry C*, 2008, 112, 10773-10777.
27. B. Subash, B. Krishnakumar, M. Swaminathan and M. Shanthi, *Langmuir*, 2012, 29, 939-949.
28. D.-H. Yoo, T. V. Cuong, V. H. Luan, N. T. Khoa, E. J. Kim, S. H. Hur and S. H. Hahn, *The Journal of Physical Chemistry C*, 2012, 116, 7180-7184.
29. Y. Zheng, L. Zheng, Y. Zhan, X. Lin, Q. Zheng and K. Wei, *Inorganic Chemistry*, 2007, 46, 6980-6986.
30. H. R. Liu, G. X. Shao, J. F. Zhao, Z. X. Zhang, Y. Zhang, J. Liang, X. G. Liu, H. S. Jia and B. S. Xu, *The Journal of Physical Chemistry C*, 2012, 116, 16182-16190.
31. D. Lin, H. Wu, R. Zhang and W. Pan, *Chemistry of Materials*, 2009, 21, 3479-3484.
32. W. Lu, S. Gao and J. Wang, *The Journal of Physical Chemistry C*, 2008, 112, 16792-16800.
33. C. Gu, C. Cheng, H. Huang, T. Wong, N. Wang and T.-Y. Zhang, *Crystal Growth & Design*, 2009, 9, 3278-3285.

34. R. Georgekutty, M. K. Seery and S. C. Pillai, *The Journal of Physical Chemistry C*, 2008, 112, 13563-13570.
35. M.-K. Lee, T. G. Kim, W. Kim and Y.-M. Sung, *The Journal of Physical Chemistry C*, 2008, 112, 10079-10082.
36. A. Tanaka, S. Sakaguchi, K. Hashimoto and H. Kominami, *ACS Catalysis*, 2012, 3, 79-85.
37. S.-i. Naya, K. Kimura and H. Tada, *ACS Catalysis*, 2012, 3, 10-13.
38. P. Li, Z. Wei, T. Wu, Q. Peng and Y. Li, *Journal of the American Chemical Society*, 2011, 133, 5660-5663.
39. L. Sun, D. Zhao, M. Ding, H. Zhao, Z. Zhang, B. Li and D. Shen, *Applied Surface Science*, 2012, 258, 7813-7819.
40. M. Misra, P. Kapur and M. L. Singla, *Applied Catalysis B: Environmental*, 2014, 150–151, 605-611.
41. D. Tsukamoto, A. Shiro, Y. Shiraishi, Y. Sugano, S. Ichikawa, S. Tanaka and T. Hirai, *ACS Catalysis*, 2012, 2, 599-603.
42. A. Zielińska-Jurek, E. Kowalska, J. W. Sobczak, W. Lisowski, B. Ohtani and A. Zaleska, *Applied Catalysis B: Environmental*, 2011, 101, 504-514.
43. L. Chen, T. Tran. T, C. a. Huang, J. Li, L. Yuan and Q. Cai, *Applied Surface Science*, 2013, 273, 82-88.
44. S. K. Ghosh and T. Pal, *Chemical Reviews*, 2007, 107, 4797-4862.
45. A. Steinbrück, A. Csáki, G. Festag and W. Fritzsche, *Plasmonics*, 2006, 1, 79-85.
46. M. Agrawal, A. Pich, N. E. Zafeiropoulos, S. Gupta, J. Pionteck, F. Simon and M. Stamm, *Chemistry of Materials*, 2007, 19, 1845-1852.
47. H. B. Michaelson, *Journal of Applied Physics*, 1977, 48, 4729-4733.
48. C.-M. Chen, C.-M. Liu, K.-H. Wei, U. S. Jeng and C.-H. Su, *Journal of Materials Chemistry*, 2012, 22, 454-461.
49. T.-H. Yang, Y.-W. Harn, K.-C. Chiu, C.-L. Fan and J.-M. Wu, *Journal of Materials Chemistry*, 2012, 22, 17071-17078.
50. S. T. Kochuveedu, D.-P. Kim and D. H. Kim, *The Journal of Physical Chemistry C*, 2011, 116, 2500-2506.

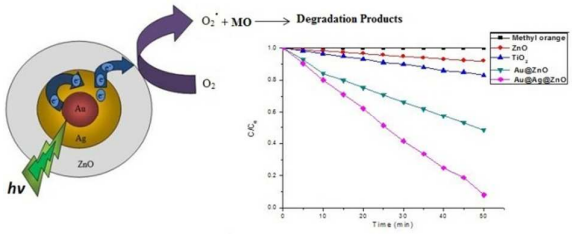

Visible light induced photocatalytic mechanism of Au@Ag@ZnO core-shell nanostructure and kinetics of methyl orange (MO) photo degradation by ZnO, Au@ZnO, Au@Ag@ZnO and TiO_2